Density Functional Calculations Modelling the Spin Density Distribution, Hyperfine Couplings, and Hydrogen Bonding Environment of the Ascorbate (Vitamin C) Free Radical

Patrick J. O'Malley

Department of Chemistry, UMIST, Manchester, M60 1QD, United Kingdom

Received: August 24, 2001

The geometry, spin density, and hyperfine couplings of the ascorbate (vitamin C) and α-hydroxytetronic acid free radicals are calculated using unrestricted B3LYP hybrid density functional calculations. Approximately 40% of the unpaired spin is found at the O2 position. The calculated ^{1}H and ^{13}C isotropic hyperfine couplings enable the sign of the experimentally determinations to be deduced and also permit the hydrogen bonding status of the free radical in aqueous solution to be described. Hydrogen bond donation is predicted to occur to the O2 and O3 atoms and leads to a significant redistribution of spin density for the free radical.

Introduction

Ascorbic acid (vitamin C) is ubiquitous to living systems, and a wide variety of biological functions have been proposed for the molecule.[1] It is widely believed to act as an antioxidant or scavenger of reactive free radicals damaging to fatty acids and nucleic acids. It is estimated that approximately 25% of reactive peroxyl free radicals are scavenged by the vitamin.[1] In cooperation with vitamin E, it has been shown to scavenge free radicals involved in lipid peroxoxidation.[2] Although structural and electronic information has been available for some time for the unoxidized form,[1] this information is not experimentally amenable for the reactive ascorbate free radical (AFR) formed by one electron oxidation. In particular, the spin density distribution of the free radical form is important as scavenging ability of antioxidants has been found to be directly related to this parameter.[3] Although the magnitude of the ^{13}C and ^{1}H hyperfine couplings (hfcs) have been available from electron paramagnetic resonance (EPR) spectroscopy studies for some time,[4] no data have been reported for ^{17}O hyperfine couplings. This lack of ^{17}O couplings plus the absence of sign information for the ^{13}C and ^{1}H couplings renders it impossible to deduce the spin density distribution of the radical. A detailed knowledge of the spin density and electronic structure of this free radical is therefore of immediate interest especially as it may hold important clues to the reactivity of the species. Both in vitro and in vivo, the free radical is generated in an aqueous environment, and hence, the effect of specific hydrogen bonding interactions between the solvent water molecules and the free radical also need to be explored.

Until recently nonempirical electronic structure studies of free radicals were extremely limited. This was a result of the poor performance of unrestricted Hartree−Fock calculations in the prediction of free radical properties. Recently, it has been demonstrated that most of the spin contamination problems encountered by unrestricted Hartree−Fock based methods are overcome by density functional approaches. In particular, there is increasing evidence that the hybrid type functionals, in particular B3LYP, have remarkable predictive power for organic free radical properties such as geometries, spin densities, hyperfine couplings and vibrational states.[5−7]

In this study, we use the B3LYP hybrid density functional method to calculate optimized geometries, spin densities, and

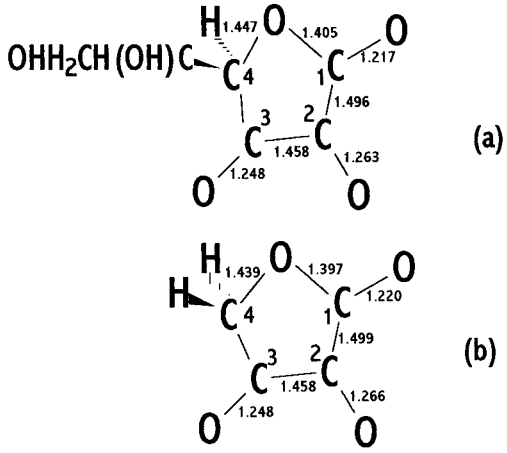

Figure 1. Comparison between calculated ring bond distances of the ascorbate (a) and α-hydroxytetronic acid (b) radicals. The overall charge for both radicals is −1. All values given in angstroms.

^{1}H, ^{17}O, and ^{13}C hyperfine couplings for the ascorbate free radical and associated models. The hydrogen bonding status of the radical in aqueous media is also probed by comparing experimentally determined hyperfine couplings with predicted values for a variety of hydrogen-bonded models.

Methods

The models used for the density functional calculations are shown in Figures 1−3. The smaller α-hydroxytetronic acid radical was used for the hydrogen bonded model calculations.

All geometries were optimized at the unrestricted B3LYP level using the EPR-II basis set utilizing the Gaussian 98[8] program. All graphical surface generation was performed using SPARTAN.[9]

Results and Discussion

The principal optimized bond distances for the full AFR radical and the models used are given in Figures 1 and 2. At this level of theory, excellent geometry predictions are expected.[5,10,11] This is borne out by Figure 3 which compares calculated bond distances for the unoxidized ascorbic acid with crystallographically determined values.[12] We can confidently

10.1021/jp013270s CCC: $20.00
Published on Web 10/18/2001

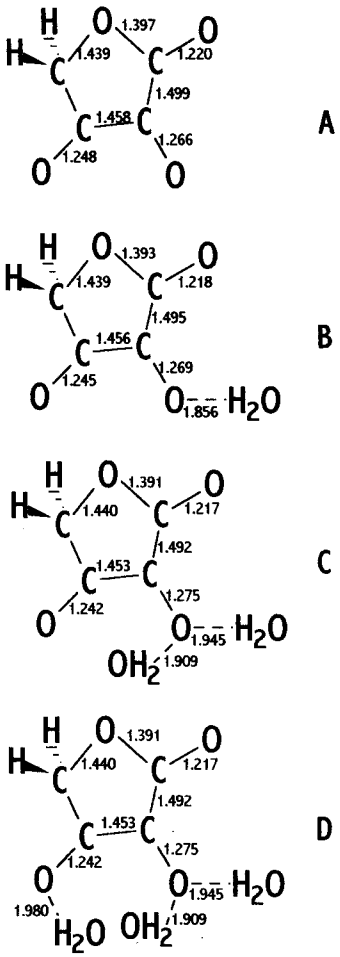

Figure 2. Optimized bond distances, angstroms, calculated for the "free" α-hydroxytetronic acid radical (A); α-hydroxytetronic acid radical with one water molecule hydrogen bonding to the O2 atom (B); α-hydroxytetronic acid radical with two water molecules hydrogen bonding to O2 (C); and α-hydroxytetronic acid radical with two water molecules hydrogen bonding to O2 and one hydrogen bonding to O3 (D). Overall charge for all complexes is −1.

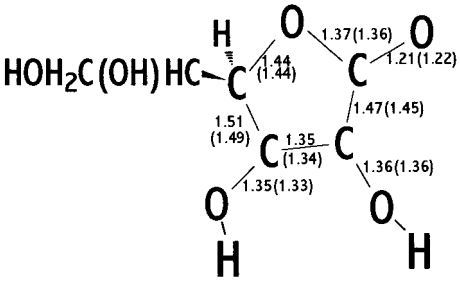

Figure 3. Comparison between ring bond distances calculated for neutral ascorbic acid and the experimentally determined ones[12] given in brackets. All values given in angstroms.

expect similar accuracy for the free radical models, where experimental structural investigations are not feasible. Figure 1 shows that minor changes in geometry are induced by including the long chain at the C4 position. Table 1 compares the isotropic hyperfine couplings calculated for the full AFR radical with those calculated for the α-hydroxytetronic acid radical. In agreement with experimental EPR studies,[4] only minor differences in the calculated ^{1}H and ^{13}C isotropic hyperfine couplings are found, suggesting an essentially identical spin density distribution for both free radicals. Because of these findings we utilize the α-hydroxytetronic acid radical only for the more time-consuming hydrogen bonded model calculations, which follow.

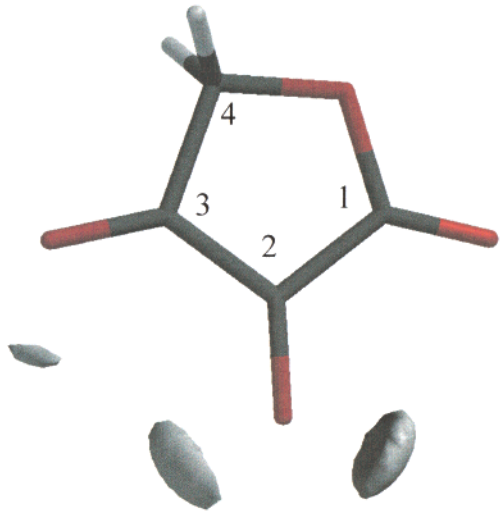

Figure 4. −150.0 kcal/mol electrostatic potential contours for the α-hydroxytetronic acid radical showing the most favorable hydrogen bond donation sites for the radical.

TABLE 1: Comparison of Calculated ^{1}H, ^{13}C, and ^{17}O Isotropic Hyperfine Couplings (G) for Ascorbate Radical and the α-Hydroxytetronic Acid Radical

position	hydroxytetronic acid radical	ascorbate radical
H4	1.8	1.5
C1	−4.4	−4.2
C2	−4.0	−4.5
C3	−3.1	−2.8
C4	−3.0	−2.7
O1	−1.8	−1.9
O2	−10.5	−10.3
O3	−5.7	−5.6
O4	−0.6	−0.6

As, both in vitro and in vivo, the free radical is generated in an aqueous environment, and hydrogen bond donation by water molecules to the electron pairs on the carbonyl oxygen atoms can be expected to occur. Because no experimental structure for the free radical is available, it is necessary to predict the most favorable sites for hydrogen bond formation. This can be done by calculating the electrostatic potential for the molecule, with hydrogen bond donation being likely at those areas of most negative electrostatic potential values. The most negative regions of electrostatic potential are shown as contour plots in Figure 4. These are located at the O2 oxygen atom closely corresponding to its lone pair electrons. In addition, a smaller region is located close to the O3 atom. We have simulated such hydrogen bonding using the models shown in Figure 2 where progressively one, two, and three hydrogen donating water molecules are added, Figure 2 parts B−D. We probe the effect of such hydrogen bonds by investigating the effect on calculated spin densities, spin populations, and hyperfine coupling values.

Comparison of experimental and calculated isotropic hyperfine coupling values for the isolated free radical A, Table 2, shows, in general, reasonable agreement between the magnitudes of the calculated and experimental isotropic hyperfine couplings. For the experimental studies only, the magnitude of the hyperfine couplings could be determined which makes it impossible to deduce the spin density distribution of the free radical. The calculated values do, of course, provide both the magnitude *and* the sign of the hfc. These calculated values indicate that the sign of the hfcs is positive for the H4 atoms

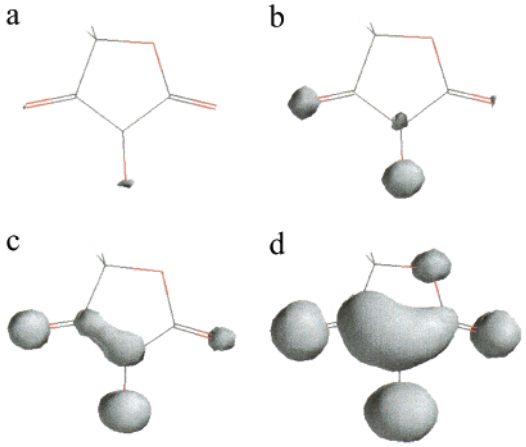

Figure 5. Unpaired spin density contour plots for the "free" α-hydroxytetronic acid radical at (a) 0.10, (b) 0.02, (c) 0.01, and (c) 0.001 e/au^3.

TABLE 2: Calculated ^{1}H, ^{13}C, and ^{17}O Isotropic Hyperfine Couplings (G) for the Model Radicals of Figure 2

position	A	B	C	D	experimental (absolute values)
H4	1.8	1.4	0.9	1.8	2.3
C1	−4.4	−5.0	−5.6	−5.6	5.7
C2	−4.0	−2.0	−0.3	−0.9	1.0
C3	−3.1	−4.0	−4.9	−3.7	3.7
C4	−3.0	−2.8	−2.6	−2.8	2.9
O1	−1.8	−1.9	−2.0	−1.9	
O2	−10.5	−10.3	−10.1	−10.2	
O3	−5.7	−5.8	−5.7	−5.5	
O4	−0.6	−0.5	−0.5	−0.4	

and negative for all of the carbon atom nuclei. It is clear from Table 2 that the most notable disagreement between calculated and experimental values occurs for the C2 position where a calculated magnitude of 4.4 G for model A compares unfavorably with the experimentally determined value of 1.0 G. The effect of progressively introducing hydrogen bond donors at the three position predicted in Figure 2 is shown also in Table 2 for models B, C, and D. Introducing one hydrogen bond donor to the O2 atom, model B, leads to a lowering in the H4 value although the magnitudes for C1, C3, C4, and in particular C2 are now in better agreement with experimental determinations. Addition of two hydrogen bond donors, model C, leads to a very significant reduction in the C2 hfc magnitude. The H4 hfc is also lowered considerably. Occupancy of the three hydrogen bonding positions, model D, appears to lead to the best agreement with experiment where the hfc magnitude for all carbon nuclei, including C2, are very close to the experimental determination.

It is clear that the hydrogen bonds can lead to significant variations in the calculated isotropic hyperfine couplings and hence must be accounted for in interpreting the experimental data. The isotropic hyperfine coupling is directly proportional to the spin density ($\alpha-\beta$) at the point of the corresponding nucleus. In a π-type system, as here, spin density arises at the nuclear positions via spin polarization or hyperconjugation.[13,14] Hence, the changes in isotropic hyperfine couplings noted in Table 2 reflect a redistribution of spin density on hydrogen bond formation. The spin density of the isolated free radical is shown at a number of contour values in Figure 5. For the high value contours, only regions of high spin density appear, whereas the lower value contours also include the less dense regions of spin. Figure 5 shows that the densest region of spin is located at the O2 atom. Significant spin density is also found at the O3 and

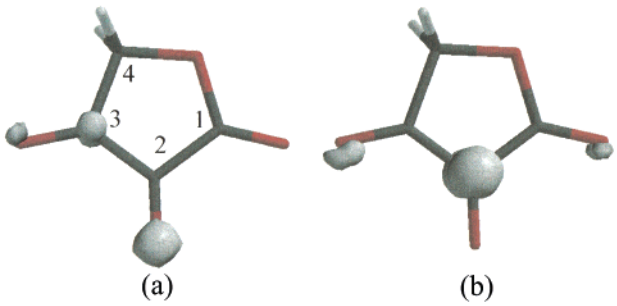

Figure 6. Difference spin density plot contour for A−C in Figure 2. (a) +0.003 and (b) −0.003 e/au^3. The apparent spin density differences near the O1 and O3 atom positions are due to slightly different geometries for the free and hydrogen bonded forms and are not related to spin density changes occurring on hydrogen bond formation.

TABLE 3: Spin Populations Calculated for the Model Radicals of Figure 2

position	A	B	C	D
C1	0.042	0.033	0.027	0.022
C2	0.158	0.201	0.236	0.216
C3	0.103	0.084	0.067	0.097
C4	0.004	0.004	0.004	0.002
O1	0.069	0.074	0.079	0.074
O2	0.390	0.366	0.348	0.358
O3	0.205	0.212	0.218	0.209
O4	0.020	0.021	0.022	0.020

TABLE 4: ^{1}H, ^{13}C, and ^{17}O Anisotropic Hyperfine Couplings (G) Calculated for the Model Radicals of Figure 2

position	A	B	C	D
C1	2.4	1.9	1.6	1.3
	−1.7	−1.5	−1.4	−1.2
	−0.7	−0.5	−0.3	−0.1
C2	9.1	11.8	14.0	12.9
	−5.7	−6.8	−7.8	−7.4
	−3.4	−4.9	−6.2	−5.6
C3	6.4	5.5	4.5	6.2
	−4.0	−3.5	−3.1	−3.9
	−2.5	−1.9	−1.4	−2.3
C4	0.4	0.4	0.4	0.4
	−0.2	−0.2	−0.2	−0.2
	−0.2	−0.2	−0.2	−0.2
O1	−7.5	−8.0	−8.5	−8.0
	3.8	4.0	4.3	4.0
	3.7	4.0	4.2	3.9
O2	−41.9	−39.4	−37.4	−38.4
	21.2	20.0	19.0	19.5
	20.7	19.4	18.4	18.9
O3	−22.3	−22.9	−23.5	−22.7
	11.3	11.6	11.8	11.5
	11.0	11.3	11.6	11.2
O4	−3.1	−3.1	−3.2	−2.7
	1.6	1.6	1.7	1.4
	1.5	1.5	1.5	1.3

C2 positions. A more quantitative estimate can be derived from the spin populations given in Table 3, which indicate that approximately 40% of the unpaired spin is located around O2. The large magnitude of the anisotropic hyperfine couplings calculated for the O2 nuclear hyperfine interaction, Table 4, is also a reflection of this large spin population as the magnitude of these couplings are directly proportional to the π spin density surrounding the nucleus.[13] From the spin populations, Table 3, it is clear that hydrogen bonding to the O2 atom leads principally to an increased spin population at the C2 position which corresponds to decreased populations at O2 (principally) and C3. This is also demonstrated in Figure 6 where a spin density difference plot (A−C) shows that a spin density increase at C2, on hydrogen bond donation, corresponds to spin density decrease

at O2 and C3. The main effect of hydrogen bond formation is a direct transfer of spin density from the O2 atom position to the C2 position. The extra positive spin (alpha) at C2 will in turn, via spin polarization, lead to a decrease in the net spin density at the C3 atom. We therefore interpret the decrease in spin density at C3 as a secondary effect. A similar spin polarization might be expected to decrease the spin population on C1 but a relatively minor decrease (compared with C3) is observed, Table 3 and Figure 6. Spin polarization can be interpreted as polarization of the paired electrons in the sigma bond by the unpaired electron present in the π orbital. Because of the exchange interaction between electrons of the same spin the distance between these electrons is smaller giving rise to an alternating polarization pattern.[13−15] The significantly longer C2C1 bond length, compared with that of C2C3, Figure 2, will be expected to considerably decrease such spin polarization. Hence, the decrease in spin density at C1 caused by hydrogen bond formation at O2 is somewhat lower than that found for C3.

The H4 hydrogens receive spin density via hyperconjugation with the C3 π spin density. Positive spin density (excess alpha) is present at C3 for all complexes, hence, giving rise to the positive value for the H4 hfc. Hydrogen bond formation to the O2 atom leads, as discussed above, however, to a lowering in the C3 spin density and hence as a result leads in a lower hfc for the H4 position, Table 2. Adding an additional hydrogen bond donor at O3, model D, reverses some of the above affects. As for hydrogen bonding at O2, hydrogen bond formation at O3 leads to a similar transfer of spin density from O3 to the C3 and to some extent reverses the effects of hydrogen bond formation at C2. The increased spin density at C3 leads in turn to a larger hfc for H4, and the effect of spin polarization by C3 on neighboring C2 leads to a decreased spin density at the C2 nucleus leading to a more negative hfc. We conclude therefore that, for the α-hydroxytetronic acid radical and by implication AFR in aqueous solution, strong hydrogen bond donation occurs as predicted by the electrostatic potential plots of Figure 2, i.e., at O2 and O3. Such a hydrogen bonding pattern is shown to lead to the best agreement between experimental and calculated isotropic hyperfine coupling values for the radical. It has been pointed out by a referee that for the full AFR radical an intramolecular hydrogen bond could be formed between the C4 chain terminal hydroxyl hydrogen, Figure 1a, and the O3 oxygen. This would be the result of a significant structural change from the structure determined for ascorbic acid.[12] If this occurred, then it is likely that that this hydrogen bonding interaction would replace that attributed to the third water molecule in our smaller model, Figure 2d. The effect of this intramolecular hydrogen bond, on spin densities and hyperfine couplings, should be very similar to that attributed to water hydrogen bond formation.

Conclusions

The geometry, spin density, and hyperfine couplings of the ascorbate free radical have been calculated using unrestricted B3LYP hybrid density functional calculations. Approximately 40% of the unpaired spin is found at the O2 position. The hydrogen bonding status of the free radical has also been probed by comparing calculated isotropic hyperfine couplings with experimental determinations. Hydrogen bond donation is predicted to occur to the O2 and O3 atoms and leads to a significant redistribution of spin density for the free radical. Because of spin polarization, this redistribution leads in turn to significant changes in the ^{13}C and ^{1}H isotropic hyperfine couplings. The spin density distribution for this radical can now be further used to explore the reactivity and scavenging activity of this radical in vivo.

References and Notes

(1) (a)Davies, M. B.; Austin, J.; Partridge, D. A. *Vitamin C: Its Chemistry and Biochemistry*; RSC Publications: U.K., 1991. (b)Bankson, D. D.; Kestin, M.; Rifai, N. *Clin. Lab. Med.* **1993**, *13*, 463.

(2) van Acker, S. A. B. E.; Koymans, L. M. H.; Bast, A. *Free Rad. Biol. Med.* **1993**, *15*, 311.

(3) van Acker, S. A. B. E.; de Groot, M. J.; van den Berg, D. J.; Tromp, M. N. J. L.; den Kelder, G. D. O.; van der Vijgh, W. J. F.; Bast, A. *Chem. Res. Toxicol.* **1996**, *9*, 1305.

(4) Laroff, G. P.; Fessenden, R. W.; Schuler, R. H. *J. Am. Chem. Soc.* **1972**, *94*, 9062.

(5) Barone, V. In *Recent Advances in Density Functional Methods*; Chong, D. P., Ed.; World Scientific Publishing: Singapore, 1995.

(6) O'Malley, P. J. *Chem. Phys. Lett.* **1996**, *262*, 797.

(7) Himo, F.; Grasslund, A.; Eriksson, L. E. *Biophys. J.* **1997**, *72*, 1556.

(8) Frisch, M. J.; Trucks, G. W.; Schlegel, H. B.; Scuseria, G. E.; Robb, M. A.; Cheeseman, J. R.; Zakrzewski, V. G.; Montgomery, J. A., Jr.; Stratmann, R. E.; Burant, J. C.; Dapprich, S.; Millam, J. M.; Daniels, A. D.; Kudin, K. N.; Strain, M. C.; Farkas, O.; Tomasi, J.; Barone, V.; Cossi, M.; Cammi, R.; Mennucci, B.; Pomelli, C.; Adamo, C.; Clifford, S.; Ochterski, J.; Petersson, G. A.; Ayala, P. Y.; Cui, Q.; Morokuma, K.; Malick, D. K.; Rabuck, A. D.; Raghavachari, K.; Foresman, J. B.; Cioslowski, J.; Ortiz, J. V.; Stefanov, B. B.; Liu, G.; Liashenko, A.; Piskorz, P.; Komaromi, I.; Gomperts, R.; Martin, R. L.; Fox, D. J.; Keith, T.; Al-Laham, M. A.; Peng, C. Y.; Nanayakkara, A.; Gonzalez, C.; Challacombe, M.; Gill, P. M. W.; Johnson, B. G.; Chen, W.; Wong, M. W.; Andres, J. L.; Head-Gordon, M.; Replogle, E. S.; Pople, J. A. *Gaussian 98*; Gaussian, Inc.: Pittsburgh, PA, 1998.

(9) Spartan, version 5.1; Wave Function, Inc.: Irvine, CA.

(10) Adamo, C.; Barone, V.; Fortunelli, V. *J. Chem. Phys.* **1995**, *102*, 1689.

(11) O'Malley, P. J. *Chem. Phys. Lett.* **1997**, *274*, 251.

(12) Hvoslef, J. *Acta Cryst.* **1968**, *B24*, 1435.

(13) Gordy, W. *Theory and Applications of Electron Spin Resonance*; Wiley: New York, 1980.

(14) Chipman, D. M. *Theor. Chim. Acta* **1992**, *82*, 93.

(15) Adamo, C.; Subra, R.; Di Matteo, A.; Barone, V. *J. Chem. Phys.* **1998**, *109*, 10244.